Polarization instability in lasers. I. Model and steady states of neodymium-doped fiber lasers

Hassina Zeghlache and Arnaud Boulnois
Laboratoire de Spectroscopie Hertzienne, Université des Sciences et Technologies de Lille 1, 59655 Villeneuve d'Ascq Cedex, France
(Received 8 August 1994)

The aim of this paper is to provide a vectorial model which can describe the dynamics of the two transverse field polarizations presented by an optical fiber laser. These dynamics are supposed to take their origin from the interaction between the propagating field and the atoms: an assumption based on the existence of a transverse distribution of dipole moments and which leads to a vectorial atomic polarization. Also, and as we have considered a frequency for each field polarization, a longitudinal dependence of the population inversion must be taken into account. A double Fourier expansion (transverse and longitudinal) of the material variables is then needed and the resulting model is analyzed using the bifurcation theory: the existence of all stationary states is fully expressed in the parameter space. The stability of these states and the system dynamic is studied in the following paper [Phys. Rev. A **52**, 4243 (1995)].

PACS number(s): 42.55.Wd, 42.65.Vh

INTRODUCTION

Polarization effects in the laser process have been analyzed for many years. The very first multimode He-Ne laser presented alternations of orthogonal linear polarization states and Zeeman lasers are known to exhibit polarized emission modes [1].

Three reasons can explain the vectorial characteristics of the output field.

(1) The first of them is related to the pump mechanisms which are supposed to give unpolarized or polarized outputs depending on the pump isotropy or anisotropy [2].

(2) The introduction of some anisotropy in the resonator, for example, Brewster windows, leads to polarized outputs.

(3) Finally the lasing medium can influence the output-state nature and especially its dynamics: crystal symmetries in solid-state lasers, for example, also provide polarized crystals.

This last reason underlies the material origin of the dynamics of the polarized field as opposed to a propagative origin: the active atoms may be uniformly (or not) distributed and fixed in the host matrix. The first and third reasons can work additively or cancel each other depending on the considered system (and thus on the interaction between light and atoms): the effect of the linearly polarized pump is to preferentially excite those atoms that are oriented in a direction close to that of the pump. However, the existence of local fields, for example, may produce an alternative output.

The earliest theoretical study introducing the spatial polarization of the active atoms mainly concerns dye-laser amplifiers [3]. These systems are characterized by anisotropic excitation mechanisms even when the pump is linearly polarized. The influence of the input-beam polarization and relative alignment polarization effects inside the active medium have also been studied by Casperson and co-workers in mode-locked dye lasers [4] and cw dye lasers [5].

In a much more complex polarization situation, one can point out a recent experimental and theoretical work that concerns the achievement of three standing waves (linear, helicoidal, and circular polarizations) in the same gas-laser system [6]. It is shown that the operating field can drastically modify the nonlinear interaction with the active medium and, as a result of that, its saturation. In conclusion, the laser dynamics can be strongly modified if one considers the interaction between the light and the active atoms in the laser process from the vectorial point of view.

The previous general discussion can be applied to the optical fiber laser (OFL) for many reasons.

(i) The absence of polarization-selective elements induces additional degrees of freedom due to the possible propagation of the two orthogonal field polarizations.

(ii) Moreover, the host silica matrix in the optical fiber is supposed to be isotropic (as long as the small stress-induced birefringence is neglected) and this allows the propagation of polarized fields.

(iii) The doping operation itself concerns ions which may produce a local field. This field induces as Stark splitting of the energy levels of the dopants and this makes several electric dipolar transitions possible. Even if the pump radiation is polarized, different pumping strengths exist: light amplification is polarization dependent, the unsaturated gain also. These polarization effects are directly related to the pump [7].

(iv) An additional and anisotropic local field can be present around the active sites: the stretching of the doped fiber may produce locally a glass structure [8]. Since both the way to produce the fiber and the doping operation are uncontrollable, this provides a variety of physical environments for the dopant ions which are responsible for different perturbing local fields. Then one can suppose that, instead of a set of identical ions, the different ranges of active atoms could be characterized by a spatial distribution of parameters depending on the host medium.

The argument for the vectorial interaction between the dopants and the propagating field is essentially based on the fact that the orientation of the lasing ions in the host matrix cannot be avoided since it has a great importance on the stimulated emission (the basic nonlinear laser process) and the system dynamics. The task of this work is to show that some interesting and experimentally already observed dy-

namics can be reproduced by a conventional laser model where we have only added the transverse orientations of the active atoms: the transverse position of the induced dipoles in the medium is expressed in a parameter.

The model we present is not exhaustive because the strict description of an OFL needs to take into account a large number of phenomena that have been neglected here, like those induced by the propagation inside the fiber, its birefringence, core ellipticity, the field diffusion on defects, etc. [9]. Some absorption and reemission mechanisms can also occur in the case of the doped fiber (in spite of the silica transparency to the pump and laser wavelengths). Other phenomena due to inhomogeneities created during the dopant insertion are neglected too: a correct description of the site-to-site differences needs the introduction of spectral inhomogeneities as well as the random orientation of the local ionic environment. These structural and mechanical imperfections are often present randomly and the disturbances they induce can couple the two polarizations: we know from Ref. [10] that, in the case of a single-mode optical fiber, the two transverse field polarizations may present fluctuating behavior. All these random or nonrandom effects will not be considered in the present paper because we think that, in the framework of the laser dynamics, they are not dominant: they can only modify the amplitude or the intensity of the interactions. All these elements justify the chosen approach for the existence of the field polarizations and their interaction via the dopants.

One more important element of our work must be emphasized. The OFL's are often used for their broad gain profile and long cavity length: a large number of longitudinal modes may oscillate essentially well above threshold. From the dynamical point of view, the modulated multimode OFL presents a variety of behaviors such as antiphase, period-doubling cascades, chaos, generalized optical bistability, etc. [11] and even without modulation these behaviors exist. From the theoretical point of view, a thousand modes cannot be usefully treated. We describe then a two-mode laser in which each mode is associated with one of the orthogonal polarization eigenstates (X and Y) and represents a subset corresponding to a cluster of longitudinal modes. Thus the multimode experimental situation is reduced to two longitudinal modes associated with the two transverse polarizations of the electric field, X and Y, and whose empty cavity frequencies are ν_x and ν_y.

Our approach is then essentially based on the interaction between light and matter [12]: the Lamb semiclassical and self-consistent formalism. The vectorial model is derived in the first part of this paper while the second part is devoted to the analysis of the steady states. The subdivisions (in four sections) leading to the full model are the following: The fields are described by Maxwell's equations, under the assumption of a plane-wave propagation (Sec. I A). The interaction between light and matter is analyzed using the Bloch equations for the density matrix elements, applied in our case to a four-level atom (Nd^{3+}) (Sec. I B 1). These equations directly give, first, the microscopic atomic polarization (Sec. I B 2) whose statistical sum leads to the source term for the propagating field and secondly the population-inversion equations (Sec. I B 3). Section I C expands the arguments for the applicability of the model to the case of Nd^{3+}-doped fiber laser: the characteristics of the active sites are detailed

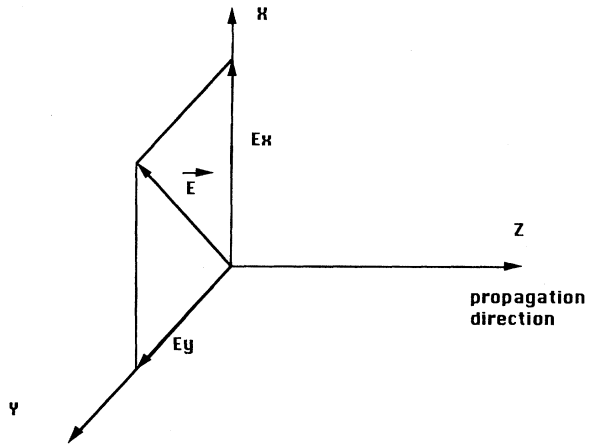

FIG. 1. The vectorial field $\vec{E}$ is in the (X,Y) plane: its components are the variables E_x and E_y and the z component is neglected.

and the concept of dipole-moment classes weighted by an angular distribution $n(\theta)$ is introduced. The final mode is given in Sec. I D where some mathematical tools like the longitudinal and angular Fourier expansions are used.

The second part of the paper is fully devoted to the steady-state solutions and their existence in the full parameter space.

We note that this work is preparatory for a second paper where more dynamical considerations will be explored using bifurcation theory and linear stability analysis.

I. VECTORIAL MODEL

A. Field equations

The laser field is governed by Maxwell's equations. Our aim is to describe the time evolution of the two modes corresponding to the X and Y polarization directions. The vectorial variables are expressed in a macroscopic frame where the X and Y axes are transverse to the Z propagation direction, as displayed in Fig. 1. The following notations are used for the total electric field:

$$\vec{E}(z,t)=\vec{E}_x(z,t)+\vec{E}_y(z,t). \tag{1.1}$$

In the OFL case, this notation is valid since the laser field propagates following the eigenmode LP_{01} (linearly polarized) whose degeneracy allows the coexistence of the two orthogonal polarizations [13].

One can write the field more precisely as

$$\vec{E}(z,t)=\tfrac{1}{2}[g_x(z)\beta_x(t)+\text{c.c.}]\vec{x}+\tfrac{1}{2}[g_y(z)\beta_y(t)+\text{c.c.}]\vec{y}, \tag{1.2}$$

where the plane-wave nature and the fast time evolution of the field are extracted following the relations

$$\beta_{x,y}(t)=E_{x,y}(t)\exp\{-i\nu_{x,y}t\}, \tag{1.3a}$$

$$g_{x,y}(z)=\exp\{ik_{x,y}z\}. \tag{1.3b}$$

The empty-cavity frequencies (or longitudinal modes) are denoted ν_x and ν_y and k_x and k_y are the corresponding wave numbers (in the plane-wave approximation).

The field equations are derived from the propagation equation. Using the slowly varying amplitude and phase approximation (SVAPA) and the "diluted media" approximation, one gets the set of equations which governs the complex amplitudes of the two field polarizations [3]:

$$(\partial_t+\kappa_x)E_x(t)=\frac{i\nu_x}{2\varepsilon_0}\frac{1}{L}\int\sum_a \eta_x(a,z,t)dz, \quad (1.4a)$$

$$(\partial_t+\kappa_y)E_y(t)=\frac{i\nu_y}{2\varepsilon_0}\frac{1}{L}\int\sum_a \eta_y(a,z,t)dz. \quad (1.4b)$$

We note the following.

(a) The source term (right-hand side) represents the statistical average of the dipole moments η induced by the laser transition. The a index stands for all the atoms' characteristics. The physical content and the notations will be specified in the next subsection which is devoted to describing the medium.

(b) The different loss coefficients (κ_x and κ_y) in the two transverse directions represent not only the passive "medium" anisotropy (fiber birefringence) but also the cavity losses due to the mirrors. These effects contribute to differentiating between the losses ($\kappa_y/\kappa_x>1$, for example). We also note that the cavity is supposed to have a ring shape which is first a convenient simplification, but a large number of Fabry-Pérot-type lasers are described by Bloch-Maxwell equations without losing their dynamical properties [7(c)].

(c) In the more precise OFL case, the longitudinal component of the mode LP_{01} can be neglected: for an index leap fiber, the field-amplitude ratio of the longitudinal component E_l (or E_z in the following) to the transverse one E_t is equal to the difference between the core and the cladding indices [13] so that $E_l/E_t=\Delta n\cong 10^{-3}-10^{-5}$.

B. Interaction between light and matter: material equations

This section is devoted to the description of the active medium. In a semiclassical model, the atom is quantified. It is described by the density matrix operator ρ which contains all the information concerning the medium state [12]. We first give the Bloch equations that govern the density matrix elements for a four-level atom (Nd^{3+}). These equations lead directly to the atomic polarization (Sec. I B 2) and the population-inversion (Sec. I B 3) equations.

1. Density-operator description of a four-level active atom

In the density matrix formalism, the average value of some observable A leads to the related macroscopic variable (and as a result, to the physical property of interest). The mean value is given by $\langle A\rangle=\mathrm{tr}\{A\rho\}$, where tr stands for the trace operation. The density matrix time evolution is governed by the Von Neumann equation

$$i\hbar\frac{\partial}{\partial t}\rho=[H,\rho], \quad (1.5)$$

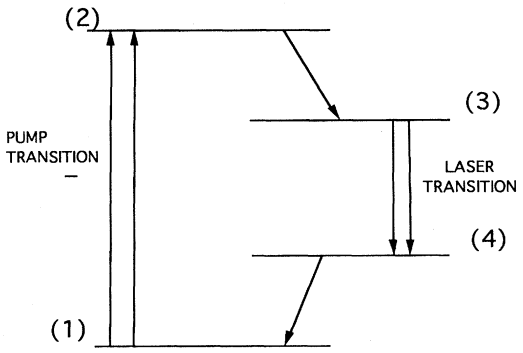

FIG. 2. The diagram which represents the four-level Nd^{3+} dopant atoms. The transitions from levels (2) and (4) are radiative.

where H is the system Hamiltonian. The Bloch equations can be derived from Eq. (1.5) where the diagonal elements represent the discrete-level normalized populations while the off-diagonal elements stand for the phase "coherence" of the transition between the two coupled levels [12].

In this paper, we shall restrict our study to neodymium as lasing atom and, in spite of its complex level structure, reduce it to only a four-level system (see Fig. 2). We do not need to directly integrate in the model the fine level structure but will suppose its existence via the absorption and gain line profiles as will be seen later. In this simplified formulation, the pump transition (being at 0.820 μm) couples the fundamental level (1) to the upper level (2) while the laser transition (occurring at around 1.08 μm) concerns two intermediate levels (3) and (4). The level (3) is metastable. Its lifetime (420 μs) is longer than those of the other levels concerned (400 ps): this allows the accumulation of atoms on it and creates a sufficient population inversion to start the laser action. The desexcitations from levels (2) and (4) produce the emission of phonons in the silica matrix via nonradiative transitions.

The Bloch equations of this four-level atom can be written in the following form [3,4]:

$$\partial_t\rho_{11}=\frac{-i}{2\hbar}(\rho_{12}\vec{\mu}_{21}\vec{E}_p-\text{c.c.})+\frac{\rho_{44}}{\tau_4}+\frac{\rho_{11}^0}{\tau_1}, \quad (1.6a)$$

$$\partial_t\rho_{22}=\frac{i}{2\hbar}(\rho_{12}\vec{\mu}_{21}\vec{E}_p-\text{c.c.})-\frac{\rho_{22}}{\tau_2}+\frac{\rho_{22}^0}{\tau_2}, \quad (1.6b)$$

$$\partial_t\rho_{33}=\frac{-i}{2\hbar}(\rho_{34}\vec{\mu}_{43}\vec{E}-\text{c.c.})+\frac{\rho_{22}}{\tau_2}-\frac{\rho_{33}}{\tau_3}+\frac{\rho_{33}^0}{\tau_3}, \quad (1.6c)$$

$$\partial_t\rho_{44}=\frac{i}{2\hbar}(\rho_{34}\vec{\mu}_{43}\vec{E}-\text{c.c.})+\frac{\rho_{33}}{\tau_3}-\frac{\rho_{44}}{\tau_4}+\frac{\rho_{44}^0}{\tau_4}, \quad (1.6d)$$

$$\partial_t\rho_{34}=-i\omega\rho_{34}-\frac{i}{\hbar}(\rho_{33}-\rho_{44})\vec{\mu}_{43}\vec{E}-\frac{\rho_{34}}{T_s}, \quad (1.6e)$$

$$\partial_t\rho_{12}=-i\omega_p\rho_{12}-\frac{i}{\hbar}(\rho_{11}-\rho_{22})\vec{\mu}_{21}\vec{E}_p-\frac{\rho_{12}}{T_p}. \quad (1.6f)$$

The notations are standard: $\vec{E}$ and $\vec{E}_p$ are respectively the oscillating and pump fields. The time T_s is the relaxation time of the lasing transition while T_p plays the same role for the pump transition. We have also defined τ_3 as the lifetime of the level (3): it characterizes essentially the spontaneous emission. The time τ_2 [τ_4] concerns the level (2) [(4)]. The frequencies ω and ω_p are the Bohr frequencies of the lasing and pump transitions. The μ_{ij} are the components of the dipole moment induced by the transition between the states i and j.

The compressed notation ρ_{ij} corresponds in fact to $\rho_{ij}(a,z,t)$: the z dependence is not of a plane-wave form as is the case for the fields [Eq. (1.3b)] because the propagation in the active medium of two fields with different frequencies induces a "grating" effect also called the "longitudinal hole burning." The a index represents all the characteristics of each active site and dopant atom in our case. The populations of the different levels relax towards their thermodynamical equilibrium value ρ^0. These values are in this case close to zero except for the ground state.

The order of magnitude of the experimental relaxation times creates a hierarchy between the variables based on their relative time scales. The numerical values used for the dopant fiber laser are then the following [14(a)]: $T_s=T_p=83$ ns; $\tau_2=\tau_4=400$ ps; $\tau_3=420$ μs. Both the coherences and the occupation of the levels (2) and (4) are fast variables compared to the fields and the occupation of the level (3). In the long-time limit (or the time scale of the slow variables), the fast variables reach their stationary value and follow adiabatically the slow variables: the fast variables are "enslaved" by the slow variables. This will be used further as an argument for simplifying the "material" equations. At this stage one can point out the theoretical and experimental work of Lacot and co-workers [14(b)] on the Er-doped fiber laser which is a class-C laser needing a coherence variable and field interaction in its description.

2. Microscopic atomic polarization

The semiclassical description of the laser effect is based on the self-consistency of the originally varying processes: assuming valid the dipolar electric approximation, the coupling between light (governed by the Maxwell equations) and matter creates microscopic electric-dipole moments whose average value is the atomic polarization. This macroscopic variable acts as a source term for the Maxwell equations [12]. The right-hand side of Eq. (1.4) is then the statistical summation of the dipole moments induced in the medium. The moments ($\langle\vec{\mu}\rangle$) are the temporal mean value of the vectorial operator $\vec{\mu}_{43}$. For one atom, the density-operator properties lead to the relation

$$\begin{aligned}\langle\vec{\mu}\rangle&=\rho_{34}(a,z,t)\vec{\mu}_{43}+\text{c.c.}\\&=\vec{\eta}_{34}(a,z,t)+\text{c.c.}\end{aligned}\tag{1.7}$$

The complex form ($\vec{\eta}_{34}$) has been chosen for notational simplicity [3,4]. Keeping the coherence in the calculations we repeat the following mathematical operations. In the macroscopic-fiber reference frame, both the optical frequencies and the plane-wave form in the X and Y directions are extracted to get

$$\begin{aligned}\vec{\eta}_{34}(a,z,t)&=\rho_{34}(a,z,t)\{\mu_x\vec{x}+\mu_y\vec{y}\}\\&=\vec{\eta}_x(a,z,t)\exp\{i(k_xz-\nu_xt)\}\\&\quad+\vec{\eta}_y(a,z,t)\exp\{i(k_yz-\nu_yt)\}.\end{aligned}\tag{1.8}$$

In all the previous formulas, the components μ_x and μ_y of the dipole moment are directly expressed in the fiber reference frame. At this stage, since the longitudinal field component is negligible ($E_z\ll E_t$) and the dipolar interaction has a scalar-product form, $\vec{\mu}\cdot\vec{E}=\mu_xE_x+\mu_yE_y+\mu_zE_z$, one can limit oneself to only the relevant transverse components of $\vec{\mu}$.

Embedded in the silica matrix, the neodymium atom has a local symmetry (of the C_{2v} group) [15]. Hence one can associate with each active atom on orthonormalized microscopic system of eigenvectors which defines axes and in this microscopic reference frame, noted down (l,m,n), the dipole moment takes the diagonal form [16]

$$\mu=\begin{pmatrix}\mu_l&0&0\\0&\mu_m&0\\0&0&\mu_n\end{pmatrix}.\tag{1.9}$$

This formulation concerns each active site and one can find as many references (l,m,n) as neodymium ions in the fiber: this makes necessary the use of the macroscopic frame (X,Y,Z) associated with the fiber and where the dipole moment can be written as

$$\begin{aligned}\mu_x&=\mu_l\langle l|x\rangle+\mu_m\langle m|x\rangle+\mu_n\langle n|x\rangle,\\\mu_y&=\mu_l\langle l|y\rangle+\mu_m\langle m|y\rangle+\mu_n\langle n|y\rangle,\\\mu_z&=\mu_l\langle l|z\rangle+\mu_m\langle m|z\rangle+\mu_n\langle n|z\rangle.\end{aligned}\tag{1.10}$$

One does not need to know all these elements to carry on the calculation. Suppose now that the norm of the projection component on the (X,Y) plane is constant and can be taken as equal to μ. In the cylindrical framework (X,Y,Z), each moment is given by

$$\begin{aligned}\mu_x&=\mu\cos\theta,\\\mu_y&=\mu\sin\theta,\end{aligned}\tag{1.11}$$

where the angle θ measures the angle of the moment (then of the atom) with respect to the X axis of the macroscopic-fiber frame and the amplitude μ appears as a fixed parameter of the atomic system (Fig. 3) while θ is still a varying parameter. This approximation is important because it assumes that the norm variations of the dipolar interaction are not the main process compared to its transverse orientation. Hence we focus on one characteristic of the whole process.

The atomic polarization term can be derived from Eq. (1.6e). An adiabatic elimination (due to the relative time scales) leads to the following expressions for each component of the moment:

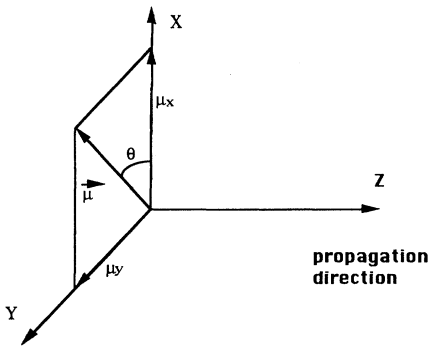

FIG. 3. The orientations of the dipole moments in the (X,Y) plane. Their amplitude is supposed constant; only θ varies.

$$\eta_x(a,z,t) = -\frac{T_s}{2\hbar}(i\alpha_x+\tilde{\alpha}_x)[\rho_{33}(a,z,t)-\rho_{44}(a,z,t)] \times\{\mu_x^2 E_x(t)+\mu_x\mu_y E_y(t) g_y(z) g_x^*(z) \times\exp[-i(\nu_y-\nu_x)t]\}, \quad (1.12a)$$

$$\eta_y(a,z,t) = -\frac{T_s}{2\hbar}(i\alpha_y+\tilde{\alpha}_y)[\rho_{33}(a,z,t)-\rho_{44}(a,z,t)] \times\{\mu_y^2 E_y(t)+\mu_x\mu_y E_x(t) g_x(z) g_y^*(z) \times\exp[-i(\nu_x-\nu_y)t]\}, \quad (1.12b)$$

where the following definitions have been used to simplify the notation:

$$\Delta_x = T_s(\omega-\nu_x), \quad \alpha_x = \frac{1}{1+\Delta_x^2}, \quad \tilde{\alpha}_x = \Delta_x\alpha_x, \quad (1.13a)$$

$$\Delta_y = T_s(\omega-\nu_y), \quad \alpha_y = \frac{1}{1+\Delta_y^2}, \quad \tilde{\alpha}_y = \Delta_y\alpha_y. \quad (1.13b)$$

The parameters Δ represent detunings between the "central" atomic frequency and the cavity frequency. A "coarse-grained" way to take into account the level fine structure and the broad emission line will be the following: values larger than one-half can be attributed to these parameters even if they are normalized to T_s and expressed in a homogeneous broadening model. This will be detailed later.

We note that the set (1.12) already shows a coupling between the two transverse components of the field; this occurs only via the medium since no direct interaction due to propagation effects inside the fiber intervenes in the description.

3. Population inversion

The population of each energy level is described by the related diagonal element of the density matrix in the set of equations (1.6). For a four-level system, one needs at least two variables and two equations (for example, the sum and the difference of the population of the levels involved in the lasing transition). However, the adiabatic elimination of the occupation of levels (2) and (4) (because of their relaxation times) reduces the system to a two-level active atom: we need only one equation for the population description [3,4]. We note this population inversion $D(a,z,t)$ and define it as $\rho_{33}(a,z,t)-\rho_{44}(a,z,t)$. It is governed by:

$$\left\{\partial_t+\frac{2}{\tau_3}\right\}D(a,z,t) = \sigma+R(a)-\frac{i}{\hbar}[\eta_x(a,z,t)E_x^*(t) + \eta_y(a,z,t)E_y^*(t)-\text{c.c}]. \quad (1.14)$$

The parameters σ and $R(a)$ represent the different pump processes. They are expressed by $\sigma=\rho_{33}^0/\tau_3-\rho_{44}^0/\tau_4$ and $R(a)=\rho_{22}/\tau_2$ and are related to the spontaneous emission and the optical pumping. The η_x and η_y are defined in Eq. (1.12). Using Eq. (1.6b) and similar definitions to those of Eqs. (1.7), (1.8), and (1.13) for the pump transition (1) to (2), the rate $R(a)$ can also be written as [3]

$$R(a) = \frac{i}{2\hbar}(\vec{\eta}_p^*\vec{E}_p-\text{c.c.})+\frac{\rho_{22}^0}{\tau_2} \cong \frac{\alpha_p T_p}{2\hbar^2}|\vec{\mu}_{21}\vec{E}_p|^2, \quad (1.15)$$

where the occupation of level (2) at thermodynamical equilibrium is neglected. The pump equations (1.6a), (1.6b), and (1.6f) are considered in the long-time limit (steady values) and the pump transition ω can be different from the Bohr frequency ω_p^0: this induces a Lorentzian pump rate due to the multiple possible pump frequencies.

Now we shall adapt the matter equations to the doped-fiber-laser case using assumptions on the doping process and its effects on the active-atom parameters.

C. Particular case of the doped fiber laser

The "material" equations (1.12) and (1.14) concern only one active site. In this section, we shall extend the description to the whole medium. This study being directly related to the spatial dependence of the atomic polarization and population inversion, it needs more details on the doped-fiber representation.

In a crystal, the position of the active sites inside the mesh can be obtained with some precision and easily generalized for the whole medium because the macroscopic variables can be integrated from the regular microscopic phenomena. Thus the electronic surroundings of the dipole moments are well established and the interaction between the matter and the propagating fields is the same for all the sites. In the fiber case, the laser environment is made up of a silica matrix which holds the active atoms and guides the fields. Silica is known as an amorphous medium. However, during the industrial process of the fiber stretching, the silica may crystallize locally [8]. This introduces privileged directions inside the fiber and breaks the disordered structure of the silica. In this description, a concept of quasiperiodic mesh can be used with a finite number of ordered structure sequences (or "eigenstructures") particular to the glass nature. These sequences repeat themselves in the medium and even when the macroscopic characteristics correspond to those of an amorphous type the microscopic sequences may be present [17]. In other words, an underlying order inside the host medium is supposed to exist which is emphasized by the dopant insertion. Indeed, the dopant atoms take up the free spaces between the SiO_2 molecules but in a suitable electronic en-

vironment the dopant position is not fully random. It may be said that the active atom tests the sites before taking its place [14,15].

It may also organize itself in "clusters" with other active atoms [15]: these "clusters" are small dopant heaps organized such that the electronic environment lets the neodymium ions escape from the host constraints. In the case of Nd atoms, these heaps have to our knowledge no contribution to the laser effect. But even if they intervene, this will be more in accordance with the atomic "organization" process rather than the random (and transversely inefficient) orientation of the dopants. Each active site (or combination "dopant-silica") interacts particularly with the fields. Then, depending on the active sites, some induced dipole orientations may be favored or forbidden. The problem is to extend the description to the whole active medium by making a discrete summation on all the dipoles.

In the material equations, the parameters and variables contain the index a which takes into account all specific characters of each active atom: the information on the induced dipole moments inside the fiber, their position, and their orientation are thus included. For the sake of simplicity, we shall follow a plane-wave model and limit the physical content of a to the efficiency of the pump and stimulated emission processes with respect to the transverse orientation of the induced dipole moments. As each induced moment has an amplitude μ and lies in the θ direction of the fiber transverse plane (with respect to the X direction), this orientation characteristic can be contained in a distribution function $n(\theta)$ allowing the passage from a discrete summation on a to an integration over the fiber volume (the active sites and more precisely the dipole orientation) leading to the macroscopic material variables. The meaning of such a distribution function could then be the following. In the fiber representation, the induced dipole being submitted to the host environment, its orientation results from a competition between the local and the applied fields. When one applies intense external fields, as in four-wave-mixing experiments generating the second harmonic, an orientation of defects is observed and then creation of a permanent polarization occurs [18]. In such experiments, the applied field imposes the orientation of the induced atomic polarization. In the laser case, on the contrary, the inverse situation predominates: the pump power being relatively weak, the competition gives the benefit to the fiber action and, although the dipoles are created by the applied fields, their orientation is strongly perturbed by the silica molecules surrounding the active site. In the quasiordered host structure, one can count a finite number of possible orientations and the concept of induced dipole classes can be applied: an angle division $d\theta$ is associated with each class and a weight $n(\theta)$ is assigned which represents the number of moments having an orientation between $\theta-d\theta/2$ and $\theta+d\theta/2$. In cylindrical coordinates, only the θ and z integrations are necessary and one obtains the following expressions for the field and population-inversion equations:

$$(\partial_t+\kappa_x)E_x(t)=\frac{i\nu_x}{2\varepsilon_0}\frac{1}{2\pi NL}\int_0^L\int_0^{2\pi}dz\ d\theta\ n(\theta)\eta_x(\theta,z,t), \tag{1.16a}$$

$$(\partial_t+\kappa_y)E_y(t)=\frac{i\nu_y}{2\varepsilon_0}\frac{1}{2\pi NL}\int_0^L\int_0^{2\pi}dz\ d\theta\ n(\theta)\eta_y(\theta,z,t), \tag{1.16b}$$

$$\left(\partial_t+\frac{2}{\tau_3}\right)\int_0^L\int_0^{2\pi}dz\ d\theta\ n(\theta)D(\theta,z,t)$$

$$=\int_0^L\int_0^{2\pi}dz\ d\theta\ n(\theta)[\sigma+R(\theta)]-\frac{i}{\hbar}\int_0^L\int_0^{2\pi}dz\ d\theta\ n(\theta)$$

$$\times[\eta_x(\theta,z,t)E_x^*(t)+\eta_y(\theta,z,t)E_y^*(t)-\text{c.c.}]. \tag{1.17}$$

The functions η_x and η_y are the atomic polarization components given by Eq. (1.12). The parameters N and L are respectively the number of active atoms and the fiber length.

The pumping coefficient can take several expressions which depend on the relative orientation of $\vec{\mu}_{21}$ and $\vec{E}_p$ [see Eq. (1.15)]. If their respective directions form with the X axis the angles θ and ψ, such that they are separated by $\theta-\psi$, the pump rate is given by

$$R(\theta)=\frac{\alpha_p T_p}{2\hbar^2}|\vec{\mu}_{21}|^2|\vec{E}_p|^2\cos^2(\theta-\psi)$$

$$=B'\cos^2(\theta-\psi)=\frac{B'}{2}\{1+\cos2(\theta-\psi)\}. \tag{1.18a}$$

Then for a linear pump polarization parallel to the X direction, ψ vanishes. Two particular cases can also be analyzed:

(i) a pump polarization oriented in the Y direction, and

$$R(\theta)=B'\sin^2\theta=\frac{B'}{2}(1-\cos2\theta), \tag{1.18b}$$

(ii) and a circular polarization (right or left) which corresponds to

$$R(\theta)=\frac{B'}{2}|\cos\theta\pm i\sin\theta|^2=\frac{B'}{2}. \tag{1.18c}$$

These pump-polarization cases will be considered separately in the following sections to analyze the different influences.

The problem to solve now is which distribution $n(\theta)$ is relevant? A complete treatment of the problem needs to number the classes and take into account each of them in the equations; this leads to a complex mathematical formulation. Thus we shall limit our analysis to soluble but still physical situations.

If one reduces the description to one dipole-moment class, the equations will correspond to the bimode ring-laser formulation (which has already been analyzed) and we lose the specific polarization property of the field [19]: the pump being linear, the output-field polarization will directly follow the dipole-moment orientation. Moreover, and from the fiber-physics viewpoint, the existence of only one direction for the moment orientation is not realistic; a strong and isotropic interaction between the active sites and the host matrix

is rare but if it happens to exist it can justify such a representation.

The opposite situation is characterized by the presence of an infinite number of classes of equivalently weighted. This corresponds to an isotropic distribution of the moments in the transverse plane: in that case $n(\theta)=N$. Such a distribution shows the domination of the local-field effects in the fiber compared to those of the applied field. Mathematically, the equations underline different terms of the Fourier series for the population inversion with respect to both θ and z. The properties of these series allow an expansion of the equations which will be exploited in the next section.

D. Transverse and longitudinal expansions of the population inversion

In this section we take advantage of the mathematical forms appearing in Eqs. (1.16) and (1.17). Using Eqs. (1.11) and (1.12) for $\eta_x(\theta,z,t)$ and $\eta_y(\theta,z,t)$, after some mathematical changes the model takes the form

$$(\partial_\tau+1)E_x(\tau)=d_x\{E_x(\tau)[D(0,0,\tau)+D(1,0,\tau)]+E_y(\tau)D^*(1,1,\tau)\}, \tag{1.19a}$$

$$(\partial_\tau+K-i\delta)E_y(\tau)=ad_y\{E_y(\tau)[D(0,0,\tau)-D(1,0,\tau)]+E_x(\tau)D(1,1,\tau)\}, \tag{1.19b}$$

$$(\partial_\tau+\gamma)D(0,0,\tau)=+\gamma\mathscr{P}^0-\gamma\{\alpha_x|E_x(\tau)|^2[D(0,0,\tau+D(1,0,\tau)]+\alpha_y|E_y(\tau)|^2[D(0,0,\tau)-D(1,0,\tau)]\}$$
$$-\frac{\gamma}{2}\{E_x(\tau)E_y^*(\tau)D(1,1\tau)d_{xy}+E_y(\tau)E_x^*(\tau)D^*(1,1,\tau)d_{xy}^*\}, \tag{1.19c}$$

$$(\partial_\tau+\gamma)D(1,0,\tau)=+\gamma\mathscr{P}^1-\gamma\{\alpha_x|E_x(\tau)|^2[D(1,0,\tau)+\tfrac{1}{2}D(0,0,\tau)]+\alpha_y|E_y(\tau)|^2[D(1,0,\tau)-\tfrac{1}{2}D(0,0,\tau)]\}, \tag{1.19d}$$

$$(\partial_\tau+\gamma)D(1,1,\tau)=-\gamma D(1,1,\tau)\{\alpha_x|E_x(\tau)|^2+\alpha_y|E_y(\tau)|^2\}-\frac{\gamma}{4}E_y(\tau)E_x^*(\tau)D(0,0,\tau)d_{xy}^*. \tag{1.19e}$$

The parameters α and $\tilde{\alpha}$ are given by Eqs. (1.13). We have used the following notations: K is the ratio between the losses of the two field polarizations ($K>1$ means less loss on the X polarization), γ is the normalized relaxation rate of the population inversions, and δ is a frequency detuning; namely,

$$K=\frac{\kappa_y}{\kappa_x},\quad a=\frac{\nu_y}{\nu_x},\quad \gamma=\frac{2}{\kappa_x\tau_3},$$

$$\delta=\frac{\nu_x-\nu_y}{\kappa_x}=(\Delta_x-\Delta_y)\frac{\gamma_\perp}{\kappa_x}, \tag{1.20a}$$

$$d_{x,y}=\alpha_{x,y}-i\tilde{\alpha}_{x,y},\quad d_{xy}=(\alpha_x+\alpha_y)+i(\tilde{\alpha}_x-\tilde{\alpha}_y). \tag{1.20b}$$

A new time scale τ is defined with respect to the losses in the X direction, following $\tau=\kappa_x t$, and this explains the normalizations of most of the dimensionless parameters to κ_x.

Reduced variables are also defined. The normalized complex fields E_x and E_y are expressed in a rotating reference frame at a pulsation ν_x/κ_x or equivalently

$$E_x(\tau)\rightarrow\sqrt{\frac{T_s\mu^2}{2\hbar^2\gamma\kappa_x}}E_x(\tau),$$

$$E_y(\tau)\rightarrow\sqrt{\frac{T_s\mu^2}{2\hbar^2\gamma\kappa_x}}E_y(\tau)\exp\left\{-i\frac{\nu_y}{\kappa_x}\tau\right\}\exp\left\{i\frac{\nu_x}{\kappa_x}\tau\right\}.$$

The dimensionless population inversion D, which is defined as $D(\theta,z,\tau)\rightarrow[\nu_x T_s\mu^2/8\hbar\varepsilon_0\kappa_x]^{-1}D(\theta,z,\tau)$, is expanded in Fourier series, transversely at order i and longitudinally at order j. The expansion coefficients $D(i,j,t)$ are detailed in Appendix A. One obtains a hierarchy of infinite equations which has to be truncated to get a closed and soluble system: we have supposed that the higher orders ($i>1$, $j>1$) of these expansions are negligible compared to the first coefficients [19]. The values of the variable $D(1,1,\tau)$ are already at the very most 10^{-2} times those of $D(0,0,\tau)$ and $D(1,0,\tau)$ which are of the same order. This will be seen in the analysis of the steady states and numerically verified for the usual laser parameters.

$\mathscr{P}^0$ and $\mathscr{P}^1$ are the two first-order terms of the pump-parameter expansion. Their evaluation is also detailed in Appendix A and depends on the experimental pump polarization. For an X pump polarization $\mathscr{P}^1=\mathscr{P}^0/2$ while for a Y pump polarization $\mathscr{P}^1=-\mathscr{P}^0/2$. In a circular pump-polarization case $\mathscr{P}^1=0$. We note that, if one supposes the existence of two variables d_x and d_y, each one contributing to one polarization direction, then D_{00} can be interpreted as d_x+d_y (or the total inversion) and D_{10} as d_x-d_y (or the "difference" inversion). In that representation and for the pump parameters $\mathscr{P}^0$ can be p_x+p_y and $\mathscr{P}^1$ the difference p_x-p_y. However, this is only an interpretation: we describe the laser process with two lasing states, but physically one deals with a single population inversion; the existence of two population inversions d_x and d_y supposes that some atoms contribute to one or other emission, which implies differentiating between active atoms. In our model (1.19) the variables and parameters appear naturally from the nonlinear interaction respecting its coherence.

Finally, one deals with a system of eight coupled real ordinary differential equations (three complex and two real). We have obtained a theoretical justification of the presence of two population inversions [11] [$D(0,0,\tau)$ and

$D(1,0,\tau)$], and also two pump parameters $\mathscr{P}^0$ and $\mathscr{P}^1$ [20]. These additional variables and parameters are often introduced phenomenologically in the medium equations while they naturally appear in this theory, directly related to the field polarizations and the underlying physics. The role of each "population inversion" will be more explicit after the analysis of the system dynamics in a second paper. However, if one can consider $D(0,0,\tau)$ as the usual population inversion between the lasing levels (which contributes to the two field polarizations), the presence of $D(1,0,\tau)$ is a signature of polarization states in matter: the variable $D(1,0,\tau)$ adds to $D(0,0,\tau)$ when it is multiplied by $E_x(\tau)$ or $|E_x(\tau)|^2$ and is subtracted from $D(0,0,\tau)$ with $E_y(\tau)$ or $|E_y(\tau)|^2$. Hence a positive sign suggests a reinforcement of the X polarization, while a negative sign will favor the Y direction. In a parametric situation which could be preferential to the X mode ($K>1$ or X-linear pump), the negative-sign situation will tend to destabilize this mode and reinforce the Y mode. These assumptions will be verified or rejected after the dynamical analyses expanded in a second paper. Finally, this model keeps the material grating due to the propagation of two field frequencies which appears via the $D(1,1,\tau)$ variable and whose role is well known essentially in the generation of the instabilities [21,19].

We shall now determine all the steady states that may be presented by the system in the whole parameter space.

II. STEADY STATES

In the long-time limit, the system reaches steady states which depend on the parameter space. They are mathematically accessible by canceling the time derivatives of the variables. The complex steady states of the fields are denoted $E_{x,y}(\tau)=\sqrt{I_{x,y}}\exp\{i\Omega_{x,y}\tau\}$. Three solutions appear.

(1) The trivial one corresponds to a laser below its threshold and then $I_x=I_y=0$, $D_{00}=\mathscr{P}^0$, $D_{10}=\mathscr{P}^1$, and $D_{11}=0$.

(2a) The monomode oscillation occurs when one polarization and only one is operating. Mathematically, there is a symmetry with respect to the losses. We call the strong mode (SM) the direction whose losses are less important (X polarization when $K>1$). In that case, the SM is characterized by the following intensities:

$$I_x=\frac{\alpha_x\mathscr{P}^0-4}{2\alpha_x}+\frac{1}{2\alpha_x}\sqrt{(\alpha_x\mathscr{P}^0-4)^2+8(\alpha_x\mathscr{P}^0+\alpha_x\mathscr{P}^1-1)}, \tag{2.1a}$$

$$I_y=0, \tag{2.1b}$$

and the frequency of the oscillating mode is

$$\Omega_x=-\Delta_x. \tag{2.1c}$$

Natural variables and parameters can be taken as

$$p^0=\alpha_x\mathscr{P}^0, \quad p^1=\alpha_x\mathscr{P}^1, \tag{2.2a}$$

$$d_0=\alpha_x D_{00s}, \quad d_{10}=\alpha_x D_{10s}, \quad \text{and} \quad I_{xs}=\alpha_x I_x, \tag{2.2b}$$

and the steady SM solution can be written as

$$I_{xs}=\frac{p^0-4}{2}+\tfrac{1}{2}\sqrt{(p^0-4)^2+8(p^0+p^1-1)}, \tag{2.3a}$$

$$I_{ys}=0, \tag{2.3b}$$

$$d_0=p^0-I_{xs}=\tfrac{1}{2}[(p^0+4)-\sqrt{C}], \tag{2.3c}$$

$$d_{10}=\frac{2p^1-I_{xs}}{2+I_{xs}}=\tfrac{1}{2}[(-p^0-2)+\sqrt{C}], \tag{2.3d}$$

$$d_{11}=0. \tag{2.3e}$$

The parameter C is defined as

$$C=(p^0-4)^2+8(p^0+p^1-1). \tag{2.4}$$

We also note the useful relation

$$d_0+d_{10}=1. \tag{2.5}$$

An increasing effective population inversion d_0 (via the pump) decreases d_{10}: the difference between the contributions to each polarization is reduced and this is favorable to the weak model (WM).

The oscillation condition for the SM ($I_x>0$) occurs when $p^0+p^1>1$ and the threshold value for the pump parameters is then

$$p^0+p^1=1. \tag{2.6}$$

For X-linear (respectively, Y-linear) pumping the X intensity (or SM) starts its oscillation with lower (respectively, higher) pump rates p^0 since p^1 is positive (respectively, negative). Moreover, and from Eq. (2.3d), we observe that the circular pump polarization ($p^1=0$) induces a steady negative d_{10} which increases the WM source terms. One can expect more complex dynamical behavior in this particular pump case.

(2b) The natural variables and parameters of the weak mode steady state appear as the following:

$$P^0=\frac{a\alpha_y}{K}\mathscr{P}^0=Q^{-1}p^0, \quad P^1=\frac{a\alpha_y}{K}\mathscr{P}^1=Q^{-1}p^1, \tag{2.7a}$$

$$D_0=\frac{a\alpha_y}{K}D_{00s}=Q^{-1}d_0, \quad D_{10}=\frac{a\alpha_y}{K}D_{10s}=Q^{-1}d_{10},$$

and

$$I_{ys}=\alpha_y I_y. \tag{2.7b}$$

The new parameter defined as

$$Q^{-1}=\frac{a\alpha_y}{K\alpha_y}=\frac{a(1+\Delta_x^2)}{K(1+\Delta_y^2)} \tag{2.8}$$

takes values around unity for reasonable values of $\Delta_{x,y}$ (between 0 and ± 0.5). It measures how far from the central atomic frequency are the two polarization frequencies: for example, $Q<1$ implies a disadvantaged X polarization (SM). However, in the second paper, we shall discuss some experimental situations which may relax this $Q\sim 1$ restriction.

The WM steady solutions are characterized by the following relations:

$$I_{ys}=\frac{P^0-4}{2}+\tfrac{1}{2}\sqrt{(P^0-4)^2+8(P^0-P^1-1)}$$

$$=\tfrac{1}{2}[(P^0-4)+\sqrt{C'}] \tag{2.9a}$$

$$I_{xs}=0, \tag{2.9b}$$

where C' is now defined as

$$C'=(P^0-4)^2+8(P^0-P^1-1). \tag{2.10}$$

The frequency of the weak-field polarization is

$$\Omega_y=K\Delta_y-\delta. \tag{2.11}$$

The population variables take the following steady values:

$$D_{00}=P^0-I_{ys}=\tfrac{1}{2}[P^0+4-\sqrt{C'}], \tag{2.12a}$$

$$D_{10}=\frac{2P^1+I_{ys}}{2+I_{ys}}=\tfrac{1}{2}[P^0+2-\sqrt{C'}], \tag{2.12b}$$

$$D_{11}=0. \tag{2.12c}$$

The weak-field polarization starts its oscillation when $P^0-P^1>1$ or $p^0-p^1>Q$, and the threshold condition for the WM is

$$P^0-P^1=1 \quad \text{or} \quad p^0-p^1=Q. \tag{2.13}$$

Some observations can be pointed out. This condition depends now on the loss ratio: the threshold increases with K. The effective pump threshold p^0 of this mode is also increased ($p^1>0$) in the case of the X-linear pump while it is decreased for a Y pump (note that the WM is the Y-direction mode when $K>1$). Finally, D_{10} is always positive above the threshold whatever the p^1 values.

The population inversions follow now:

$$D_{00}-D_{10}=1 \quad \text{or} \quad d_0-d_{10}=Q, \tag{2.14}$$

and one can notice the negative role of d_{10} for the WM since it increases with d_0.

These two monomode fields can never oscillate simultaneously and in a stable way: when a parameter is varied the system can switch from one steady state to the other via a steady bifurcation. Thus even in regions of the parameter space where these two steady states may coexist the system will select one of them depending on the attraction basin (or initial conditions).

(3) A bimode solution is also present in the system. We get it in seeking for solutions of the form $E_{x,y}(\tau)=E_{xs,ys}\exp\{i\Omega_{x,y}\tau+\phi_{x,y}\}$ for the fields, and $D_{11}(\tau)=\mathscr{A}_{11}\exp\{i\Omega_D\tau+\phi_D\}$, $D_{00}(\tau)=\mathscr{A}_0$, $D_{10}(\tau)=\mathscr{A}_{10}$ for the population inversions. The ϕ's are the initial phases of the complex variables. The existence of such a steady solution requires the following relation to be satisfied (solvability condition):

$$\Omega_D=\Omega_y-\Omega_x. \tag{2.15}$$

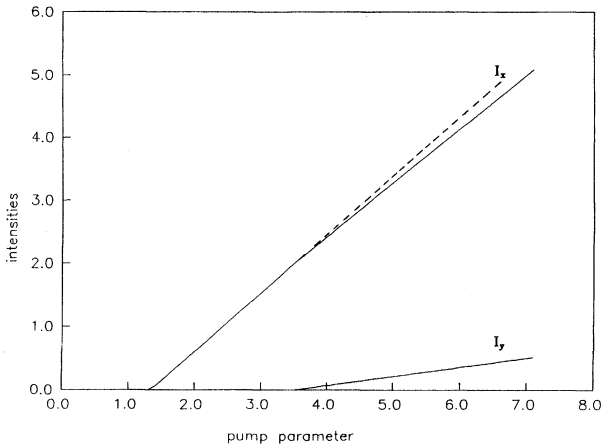

FIG. 4. Bifurcation diagram representing the OFL steady states versus the bifurcation parameter $\mathscr{P}^0$. The system is stable on the full lines. The dashed lines correspond to the continuation of the SM solution which becomes unstable. The parameters are $\Delta_x=1.0$, $\Delta_y=0.0$, $\delta=0.01$, $a=K=1.0$, $\gamma=0.001$, and $\mathscr{P}^1=\mathscr{P}^0/2$.

One can lay down the definitions

$$\phi=\phi_x+\phi_D-\phi_y, \tag{2.16a}$$

$$h=\alpha_x+\alpha_y \quad \text{and} \quad h'=\Delta_x\alpha_x-\Delta_y\alpha_y, \tag{2.16b}$$

$$I=1+I_{xs}+I_{ys}=1+\alpha_xE_{xs}^2+\alpha_yE_{xs}^2$$

$$=-\frac{\Omega_D}{\gamma}\frac{h\cos\phi+h'\sin\phi}{h\sin\phi-h'\cos\phi}=\text{const.} \tag{2.16c}$$

where the last equation appears as a conservative law for the intensities: it expresses the fact that when a parameter is varied an increasing intensity of one polarization necessarily induces a decreasing of the other one. This feature is represented in Fig. 4, where we have plotted the steady-state intensities versus the pump parameter p^0. The X polarization starts oscillating around unity pumpings and the bimode at 3.5: the X intensity falls progressively as soon as the Y intensity increases. For the displayed case, the X-linear pump is considered and the parameters are $a=1.0$, $K=1.0$ (or symmetric losses), $\gamma=0.001$, $\delta=0.01$, $\Delta_y=0.0$, and $\Delta_x=1.0$.

The steady bimode solution is characterized by the following relations for the inversions where the notations (2.2) of the strong mode have been used:

$$d_{11}=\alpha_x\mathscr{A}_{11}=-\frac{h\cos\phi+h'\sin\phi}{4I}E_{xs}E_{ys}d_0, \tag{2.17a}$$

which supposes $\tan\phi>-h/h'$ to get a d_{11} positive amplitude: the phases are not arbitrary and the solution is phase locked,

$$Id_{10}=p^1-\frac{I_{xs}-I_{ys}}{2}d_0 \tag{2.17b}$$

and the variable d_0 satisfies

$$d_0\left\{I-\frac{(I_{xs}-I_{ys})^2}{2I}-\frac{(h\cos\phi+h'\sin\phi)^2}{\alpha_x\alpha_y}\frac{I_{xs}I_{ys}}{4I}\right\}$$

$$=p^0-p^1\frac{I_{xs}-I_{ys}}{I}. \quad (2.17c)$$

The amplitudes of the output fields are then solutions of

$$1=(d_0+d_{10})-I_{ys}\frac{h\cos\phi+h'\sin\phi}{4I\alpha_y}d_0(\cos\phi+\Delta_x\sin\phi), \quad (2.18a)$$

$$Q=(d_0-d_{10})-I_{xs}\frac{h\cos\phi+h'\sin\phi}{4I\alpha_x}d_0(\cos\phi-\Delta_y\sin\phi), \quad (2.18b)$$

while the frequencies are given by

$$\Omega_x=\Delta_x(d_0+d_{10})-\frac{I_{ys}}{\alpha_y}\frac{h\cos\phi+h'\sin\phi}{4I}d_0(-\sin\phi+\Delta_x\cos\phi), \quad (2.19a)$$

$$\Omega_y=-\delta+KQ^{-1}\Delta_y(d_0-d_{10})-KQ^{-1}\frac{I_{xs}}{\alpha_x}\frac{h\cos\phi+h'\sin\phi}{4I}d_0(\sin\phi+\Delta_y\cos\phi), \quad (2.19b)$$

$$\Omega_D=-\gamma I\frac{h\sin\phi-h'\cos\phi}{h\cos\phi+h'\sin\phi}. \quad (2.19c)$$

This last equation is identical to (2.16c). The general solution of the system (2.17) and (2.19) is not easy to obtain analytically even if the method is straightforward. One gets a second-order polynomial for the intensity I_{xs} using the conservative character of the intensities (which represents in fact a function of the frequency Ω_D). Then via I one has access to I_{ys} and all the other variables (still versus Ω_D). The Ω_D equation (2.19c) leads to a polynomial equation for Ω_D that solves the problem fully while the compatibility condition (2.15) is finally utilized to fix the combined phase ϕ. The formulas are complicated and cannot be explored in the parameter space: we shall not present them here. However, in Appendix B some elements of these calculations will be expanded in a perturbative case corresponding to a small γ expansion: the bimode solution is obtained, especially its threshold, and this can be related to the stability analysis detailed in a second part of this work.

As a confirmative element of the role of the variables and a matter of discussion, we show in Figs. 5(a) and 5(b) two cases of possible behaviors versus two parameters ($\mathscr{P}^0$ and Δ_x), obtained by a direct integration of the set (1.19) and for a realistic parametric situation [$\Delta_y=0.5$, $\delta=0.001$, $a=K=1.0$, $\gamma=0.001$, and $\mathscr{P}^1=0.0$ for Fig. 5(a), and $\mathscr{P}^1=\mathscr{P}^0/2$ for Fig. 5(b)] corresponding to respectively circular (a) and linear pump polarization (b).

The observations confirm the previous analyses: as an example, for a fixed detuning Δ_x favorable to the SM and thus less than Δ_y, the system first switches on the SM monomode output and then as the pump intensity is increased it starts

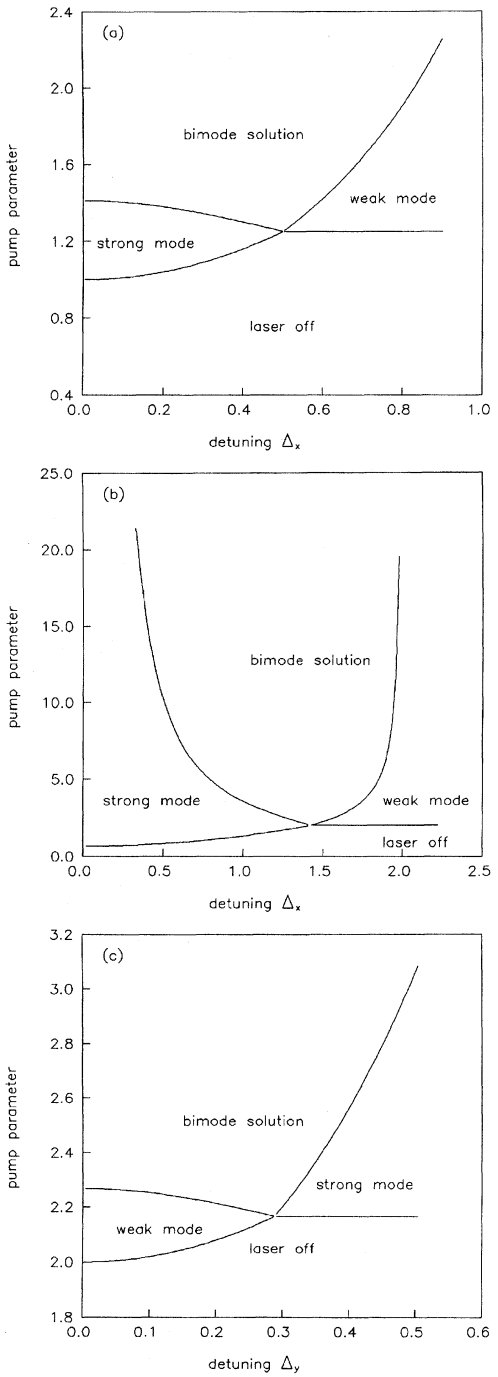

FIG. 5. Steady states derived from a direct integration of the system (1.19) versus the pump P^0 and Δ_x for the parametric situation $\Delta_y=0.5$, $\delta=0.001$, $a=K=1.0$, $\gamma=0.001$, and (a) $\mathscr{P}^1=0.0$, which means a circular, and (b) $\mathscr{P}^1=\mathscr{P}^0/2$, a linear pump polarization, while (c) is the same as (a) and (b) but versus Δ_y and for $\mathscr{P}^1=\mathscr{P}^0/2$, $\Delta_x=1.5$.

oscillating on the bipolarized solution. In contrast, when $\Delta_y<\Delta_x$ the WM oscillates first. The WM threshold is higher valued compared to the SM threshold and the bimode operation follows the same rule: "large detunings" means less probability for atomic emission (with respect to the emission

gain line) and hence need more pumping to realize the oscillation. Comparing the two figures 5(a) and 5(b), one can say that the X-linear pump [case 5(b)] presents a stronger stability with respect to the monomode oscillation: the operating thresholds are lower and larger pumpings are needed to start the bimode oscillation. We also note that larger detunings Δ_x are necessary to realize the WM oscillation: the intersection point corresponds to $Q=1$ (or equal detunings) in Fig. 5(a) while Q is much lower ($\Delta_x > \Delta_y$) in Fig. 5(b). The stabilizing effect on the X mode due to the nonzero (and positive) value of P^1 (and then of D_{10}) is more effective when the pump is X linear rather than circular. However, for large Δ_x detunings, the WM oscillation still occurs.

We must make clear that the direct integration includes the stability characteristics of the solution: versus Δ_x and for a fixed pump parameter, one can observe that the SM is stable below the intersection point, while the WM is stable above it. This is just the contrary if one studies the system versus Δ_y as presented in Fig. 5(c). In this case, one has to take a large enough Δ_x detuning (around 1.5) to ensure that an existence domain of the WM exists. The worse pump condition for WM oscillation, the X-linear pump, is considered. In the case of a circular polarization, Δ_x around 0.5 is enough to allow a WM oscillation. These comments show the counterbalanced effect of two parameters such as the detunings and the pump rates which describe the competition between their originating processes: the broadened emission and the nature of the pumping. These stability conclusions will be confirmed in a second paper.

CONCLUSION

We have presented a vectorial model describing a laser for which the simultaneous oscillation of the two transverse field polarizations is realized. This dynamic is supposed to have a "material origin": the atomic polarization is transversely polarized so that the nonlinear interaction between light and active atoms is modified. This choice of formulation follows the observation of an experimental dynamical behavior governed by the population inversion (also called population dynamics). In this way and far from phenomenological modeling, a theoretical justification for the presence of two "population inversions" [$D(0,0,\tau)$ and $D(1,0,\tau)$] and also two pump parameters $\mathscr{P}^0$ and $\mathscr{P}^1$ has been derived even if we deal with assimilated "two-level" atoms. The calculations have been expanded for the simplified case of spatial isotropic distribution of the dipole-moment orientation. Nevertheless, the steady solutions presented by the model and the number and the role of the system variables confirm qualitatively the main steady features presented by the OFL.

One needs now to explore the stability of these steady states and to go further in the study of the dynamical behaviors presented by this model, the goal being a comparison with the experimental observations. A second paper will be devoted to linear stability analysis using the bifurcation theory. This asymptotic study measures, in the immediate neighborhood of the variables, the differences induced by a small perturbation. The parameter space will be analytically explored as far as possible in terms of the system dynamics.

ACKNOWLEDGMENTS

The authors wish to thank Professor P. Glorieux, Dr. D. Derozier, and Dr. S. Bielawski for fruitful discussions and their encouragements to pursue this work. The Laboratoire de Spectroscopie Hertzienne is both a university laboratory and associated with the CNRS (URA 249).

APPENDIX A: FOURIER EXPANSION OF POPULATION INVERSION AND RELATED PUMP PARAMETERS

In its final form, the model presents two pump parameters and three population-inversion variables. The aim of this Appendix is to outline their origin.

The pump parameter is related to the $[\sigma+R(\theta)]$ term in Eq. (1.17). The first contribution is due to occupation of levels (3) and (4) at thermodynamic equilibrium while the more relevant second term is the optical pumping and thus depends on the polarization direction. Replacing the $\eta_{x,y}(a,z,t)$ (1.12) in the set (1.17) gives two nonlinear contributions of the form $\cos^2\theta E_x+\cos\theta\sin\theta E_y\exp[i(k_y-k_x)z]$ and $\sin^2\theta E_y+\cos\theta\sin\theta E_x\exp[-i(k_y-k_x)z]$.

The exponential terms suggest Fourier expansion versus the longitudinal z coordinate, the $\cos^2\theta$ (or $\sin^2\theta$) terms are transformed to $\cos 2\theta$, and the $\cos\theta\sin\theta$ term to $\sin 2\theta$: terms of transverse expansion appear. Thus in this problem two parallel series are needed. When it is applied to the population inversion this mathematical tool leads to the coefficients $D(i,j,t)$ and only three components of the expansion are necessary (and kept) in our model. At order (0,0) in θ and z, one obtains

$$D(0,0,\tau)=\frac{1}{2\pi NL}\int_0^L\int_0^{2\pi} dz\, d\theta\, n(\theta)D(\theta,z,\tau). \quad \text{(A1)}$$

at the first order in θ and zeroth in z one has

$$D(1,0,\tau)=\frac{1}{2\pi NL}\int_0^L\int_0^{2\pi} dz\, d\theta\, n(\theta)D(\theta,z,\tau)\cos 2\theta, \quad \text{(A2)}$$

and finally the order unity in both θ and z is the following:

$$D(1,1,\tau)=\frac{1}{2\pi NL}\int_0^L\int_0^{2\pi} dz\, d\theta\, n(\theta)D(\theta,z,\tau)\sin 2\theta \times\exp\{-i(k_y-k_x)z\}. \quad \text{(A3)}$$

When $n(\theta)=N$, $D(0,0,\tau)$ is the normal averaged population inversion between the lasing levels, while $D(1,0,\tau)$ is the effective transfer population inversion between the two transverse directions: it represents the existence of polarized states in the medium. $D(1,1,\tau)$ is essentially the longitudinal grating due to the propagation of two frequencies.

For the pump parameters, only their angle dependence is considered (which is probably a strong approximation) and so only the θ expansion is needed. One can easily show that only the two following orders:

$$\mathscr{P}^0=\frac{\nu_x T_s\mu^2}{8\hbar\varepsilon_0\gamma\kappa_x}\int_0^{2\pi} d\theta\, n(\partial)[\sigma+R(\theta)], \quad \text{(A4)}$$

$$\mathscr{P}^1=\frac{\nu_x T_s \mu^2}{8\hbar\varepsilon_0\gamma\kappa_x}\int_0^{2\pi} d\theta\, n(\theta)[\sigma+R(\theta)]\cos 2\theta \quad \text{(A5)}$$

appear naturally in the equations.

The optical pumping $R(\theta)$ is given by Eqs. (1.18) which can be summarized in the following way:

$$R(\theta,\psi)=\frac{B'}{2}\{1+\cos 2(\theta-\psi)\} \quad \text{(A6a)}$$

to take into account the ψ-linear transverse polarization of the pump, or for the X-, or Y-linear pump and circular pump:

$$R(\theta)=\frac{B'}{2}(1+n\cos 2\theta), \quad \text{(A6b)}$$

where n is respectively $+1,-1$, and 0.

In the case of an isotropic distribution of dipole moments and defining the coefficients A and B such that

$$A=\frac{\nu_x T_s \mu^2}{4\hbar\varepsilon_0\gamma\kappa_x}\sigma \quad \text{and} \quad B=\frac{\nu_x T_s \mu^2}{8\hbar\varepsilon_0\gamma\kappa_x}B' \quad \text{(A7)}$$

the two first-order pump parameters reduce to

$$\mathscr{P}^0=\left(A+\frac{B}{2}\right)\frac{1}{2\pi N}\int_0^{2\pi} d\theta\, n(\theta), \quad \text{(A8)}$$

$$\mathscr{P}^1=n\,\frac{B}{2}\,\frac{1}{2\pi N}\int_0^{2\pi} d\theta\, n(\theta)\cos^2 2\theta, \quad \text{(A9)}$$

where N is the total number of active atoms. Therefore, and because of the $n(\theta)$ choice, $\mathscr{P}^0$ is the θ-independent term (or the effective pump) while $\mathscr{P}^1$ contains the pump contributions to the dipole moment directions (θ).

(a) In the case of an X-linear pump, $n=1$, one easily obtains

$$\mathscr{P}^0=A+\frac{B}{2} \quad \text{and} \quad \mathscr{P}^1=\frac{B}{4}.$$

At thermodynamic equilibrium, the levels are generally little populated, the spontaneous emission contribution and the parameter A are negligible, and one obtains the relation $\mathscr{P}^1=\frac{1}{2}\mathscr{P}^0$. The threshold value of the SM (X-polarization oscillation) is $p^0=\frac{2}{3}$ while for the WM its value is higher: $P^0=Q^{-1}p^0=2$.

(b) In the case of a Y-linear pump ($n=-1$) one gets

$$\mathscr{P}^0=A+\frac{B}{2} \quad \text{and} \quad \mathscr{P}^1=-\frac{B}{4}.$$

At thermodynamic equilibrium, $\mathscr{P}^1=-\frac{1}{2}\mathscr{P}^0$. The threshold condition for the SM becomes $p^0=2$ and for the WM (the Y direction) the oscillation starts when $P^0=Q^{-1}p^0>\frac{2}{3}$.

(c) For a circular pump polarization, $\mathscr{P}^1=0$ and the pump contribution to each polarization is equal. The threshold condition for the SM becomes $p^0=1$ and for the WM (the Y direction) the oscillation occurs when $P^0=Q^{-1}p^0>1$.

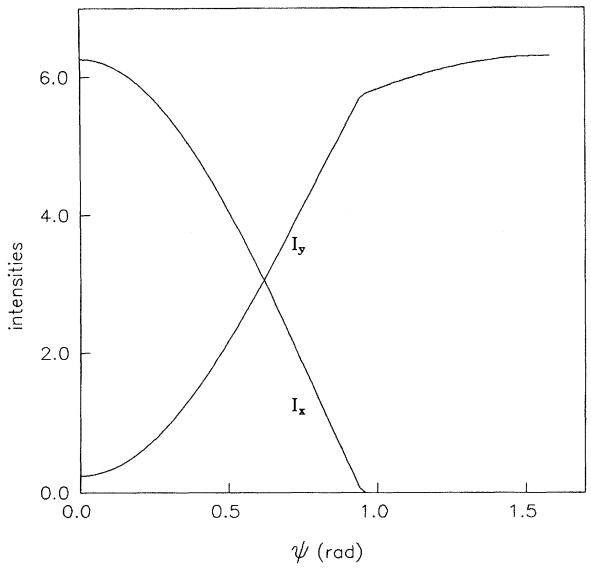

FIG. 6. The bimode intensities are plotted versus the angle ψ of the linearly polarized pump with the X axis for the parametric situation $\mathscr{P}^0=8$, $\Delta_x=0.9$, $\Delta_y=0.1$, $\delta=0.01$, $a=K=1.0$, and $\gamma=0.09$.

In the second paper, we shall consider only the cases (a) and (c). The relation between the cases (a) and (b) is evident when one observes Fig. 6: this graph gives the intensities of two polarizations versus the angle ψ of a ψ-linear pump for which $\mathscr{P}^0=A+B/2$ (taken around 8) and $\mathscr{P}^1=(B/4)\cos 2\psi$. In that case the thresholds of the SM and WM are respectively given by

$$(\mathscr{P}^0+\mathscr{P}^1)_{\text{thr}}=1/\alpha_x \quad \text{and} \quad (\mathscr{P}^0-\mathscr{P}^1)_{\text{thr}}=K/a\alpha_y \quad \text{(A10)}$$

and one can see from these formulas that the WM threshold directly increases when the loss ratio increases while the SM's is independent [7(b)]. In Fig. 6 the parametric situation is $\Delta_x=0.9$, $\Delta_y=0.1$ (the Y-polarization oscillation is advantaged), $\delta=0.01$, $a=K=1.0$, and $\gamma=0.09$. We have plotted the two steady bimode polarization intensities versus the angle ψ of the linearly polarized pump and the X axis of the fiber. The values of the intensities are somewhat cosine (sine) related to the angle ψ [7,20]: the asymmetry of the curves is due to the detunings.

APPENDIX B: THE BIPOLARIZED STEADY OSCILLATION

The system (2.5) and (2.19) can give us more information about the bimode oscillation in the particular but real situation where $\gamma\ll 1$. We start the calculation by imposing the following necessary requirements: the steady values of I_{xs}, I_{ys}, d_0, and d_{10} are of order unity in the small-γ expansion, while d_{11} is taken as $o(\gamma)$.

Following Eq. (2.17a) the lowest order of the combined phase is fixed: $h\cos\phi^{(0)}+h'\sin\phi^{(0)}=0$, and the phase is locked such that

$$\tan\phi^{(0)}=-\frac{\alpha_x+\alpha_y}{\Delta_x\alpha_x-\Delta_y\alpha_y}\,. \tag{B1}$$

The symmetric case ($\Delta_x=\Delta_y$) corresponds to a $\pi/2-\phi^{(0)}$ phase.

From the zeroth order of Eq. (2.18), one easily gets the real "inversions" as

$$d_0^{(0)}=(Q+1)/2 \quad \text{and} \quad d_{10}^{(0)}=(1-Q)/2, \tag{B2}$$

while $d_{11}^{(0)}$ evidently cancels [since it is an $o(\gamma)$ term]: this confirms the truncation of the infinite longitudinal Fourier series to this order.

The intensities are then derived from Eqs. (2.71b) and (2.17c) and are given by

$$I_{xs}^{(0)}=-\frac{1}{2}+\frac{(1-3Q)p^0-4Qp^1}{Q^2-6Q+1}\,, \tag{B3a}$$

$$I_{ys}^{(0)}=-\frac{1}{2}+\frac{(Q-3)p^0+4p^1}{Q^2-6Q+1}\,. \tag{B3b}$$

The simultaneous existence of the two polarization intensities is governed by the following inequalities:

$$(1-3Q)p^0-4Qp^1\geqslant\frac{Q^2-6Q+1}{2}\,, \tag{B4a}$$

$$(Q-3)p^0+4p^1\geqslant\frac{Q^2-6Q+1}{2}\,. \tag{B4b}$$

For a linear pump polarization, these inequalities take the form

$$p^0\geqslant\frac{Q^2-6Q+1}{2(1-5Q)}\,, \tag{B5a}$$

$$p^0\geqslant\frac{Q^2-6Q+1}{2(Q-1)}\,, \tag{B5b}$$

while in a circular-polarization situation one gets

$$p^0\geqslant\frac{Q^2-6Q+1}{2(1-3Q)}\,, \tag{B6a}$$

$$p^0\geqslant\frac{Q^2-6Q+1}{2(Q-3)}\,. \tag{B6b}$$

The systems (B6) and (B5) are represented by Figs. 7(a) and 7(b), respectively, around their intersection points ($Q_i=\frac{1}{3}$ and 1, respectively). These figures correspond to Figs. 5(a) and 5(b) which are obtained by a direct integration of the system of differential equations (1.19) and are given versus the parameter Δ_x. One can notice, however, that for $Q<Q_i$ the existence of the bimode solution is governed by the Y-polarized oscillation (B4b) while above the intersection point it is the X polarization that fixes this existence limit. We have also reported on the same graph the monomode thresholds [large- (WM) and small- (SM) dashed line]. At this stage, one cannot say which mode is stable. However, keeping in mind the definition of

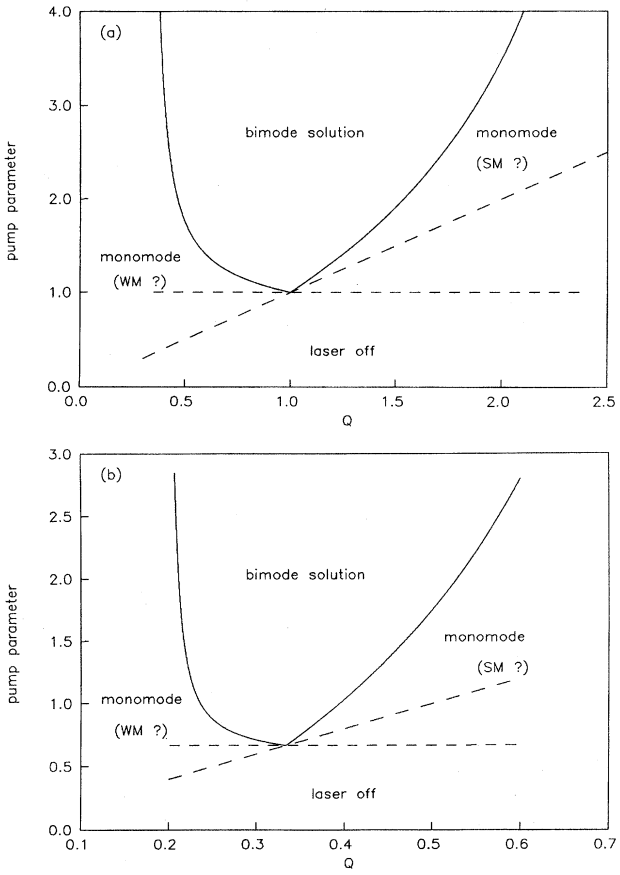

FIG. 7. Same as Fig. 5 with (a) $\mathscr{P}^1=0$ (circular pump polarization) and (b) $\mathscr{P}^1=\mathscr{P}^0/2$ (linear pump polarization) obtained with the asymptotic Eqs. (B6) and (B5), respectively. The full lines correspond to the bimode existence domain while the large-dashed lines are the WM threshold and the small-dashed lines the SM threshold.

$Q[=K(1+\Delta_y^2)/a(1+\Delta_x^2)]$, an increasing Δ_x induces a decrease in Q, so that one can suspect the WM to be stable for $Q<Q_i$. The linear stability analysis in a second paper will provide more information.

From the point of view of frequencies, one easily gets

$$\Omega_x^{(0)}=\Delta_x \quad \text{and} \quad \Omega_y^{(0)}=-\delta+K\Delta_y\,, \tag{B7}$$

while

$$\Omega_D^{(0)}=\Omega_y^{(0)}-\Omega_x^{(0)}=\{1+I_{xs}^{(0)}+I_{ys}^{(0)}\}\frac{1}{\phi^{(1)}}\,. \tag{B8}$$

This last equation leads to the combined-phase first-order correction and contributes to the next order. The inversions are given by

$$d_{11}^{(1)}=\frac{\pm\sqrt{h^2+h'^2}}{8(\delta-K\Delta_y+\Delta_x)}(Q+1)E_{xs}^{(0)}E_{ys}^{(0)}\,, \tag{B9}$$

$$d_0^{(1)}=\frac{h'^2-h^2}{h^2+h'^2}\frac{Q+1}{16(-\delta+K\Delta_y-\Delta_x)}\{(I_{xs}^{(0)}+I_{ys}^{(0)})(\Delta_x-\Delta_y)$$
$$-2(\alpha_y\Delta_y I_{xs}^{(0)}-\alpha_x\Delta_x I_{ys}^{(0)})\}, \quad \text{(B10)}$$

$$d_{10}^{(1)}=\frac{h'^2-h^2}{h^2+h'^2}\frac{Q+1}{16(-\delta+K\Delta_y-\Delta_x)}\{2(\alpha_y\Delta_y I_{xs}^{(0)}+\alpha_x\Delta_x I_{ys}^{(0)})$$
$$-(I_{xs}^{(0)}-I_{ys}^{(0)})(\Delta_x-\Delta_y)\}. \quad \text{(B11)}$$

The corrections to the intensities are then given by the following linear set of equations for $x=I_{xs}^{(1)}+I_{ys}^{(1)}$ and $y=I_{xs}^{(1)}-I_{ys}^{(1)}$:

$$2x\{1-Q\}+y\{1+Q\}=-4x^{(0)}d_{10}^{(1)}-2y^{(0)}d_0^{(1)}, \quad \text{(B12a)}$$

$$x\{(Q+1)(2x^{(0)2}+y^{(0)2})-4p^1y^{(0)}\}+Y\{4p^0x^{(0)}-2x^{(0)}y^{(0)}$$
$$\times(1+Q)\}=-8x^{(0)}\frac{d_0^{(1)}}{(Q+1)}\{p^0x^{(0)}-p^1y^{(0)}\}, \quad \text{(B12b)}$$

where $x^{(0)}=1+I_{xs}^{(0)}+I_{ys}^{(0)}$ and $y^{(0)}=I_{xs}^{(0)}+I_{ys}^{(0)}$ are known.

The calculation to this and further orders does not give any interesting and complementary information on this bimode solution.

[1] W. Culshaw and J. Kannelaud, Phys. Rev. **145**, 257 (1966); **156**, 308 (1967); A. Le Floch, G. Ropars, J. M. Lenormand, and R. Le Naour, Phys. Rev. Lett. **52**, 918 (1984); A. Le Floch, G. Ropars, and R. Le Naour, Europhys. Lett. **3**, 695 (1987); A. P. Voitovitch, L. P. Svirina, and V. N. Severikov, Opt. Commun. **80**, 435 (1991), and references therein.

[2] B. I. Stepanov and V. P. Gribkovskii, *Theory of Luminescence* (Ihffe Books, London, 1968).

[3] K. C. Reiser and L.W. Casperson, J. Appl. Phys. **51**, 6075 (1980); **51**, 6083 (1980).

[4] S. H. Jiang and Lee W. Casperson, J. Appl. Phys. **69**, 1866 (1991); Lee W. Casperson, *ibid.*, **69**, 8005 (1991).

[5] L. W. Casperson, W. J. Sandle, A. C. Wilson, D. M. Warrington, and R. J. Ballagh, J. Appl. Phys. **69**, 8005 (1991).

[6] F. Bretenaker and A. Lefloch, Phys. Rev. A **43**, 3704 (1991).

[7] (a) E. Delvaque, Ph.D. thesis, Centre National d'Etudes en Telecommunications Lannion and University of Lille, 1993; (b) R. Leners, P. L. Francois, and G. Stéphan, Opt. Lett. **19**, 275 (1994); (c) R. Leners, Ph.D. thesis, CNET Lannion, 1994.

[8] P. W. France, *Optical Fiber Lasers and Amplifiers* (CRC, London, 1991).

[9] M. Monerie and L. Jeunhomne, Opt. Quantum Electron. **12**, 449 (1980).

[10] Tiang Feng, Wu Yizun, and Ye Peida, IEEE J. Light Technol. **8**, 1235 (1990).

[11] S. Bielawski, D. Derozier, and P. Glorieux, Phys. Rev. A **46**, 2811 (1992); Opt. Commun. **83**, 97 (1991).

[12] M. Sargent III, M. Scully, and W. E. Lamb, Jr., *Laser Physics* (Addison-Wesley, Reading, MA, 1974), and references therein.

[13] G. P. Agrawal, *Nonlinear Fiber Optics* (Academic, New York, 1989), p. 32.

[14] (a) M. Le Flohic, P. L. François, and G. M. Stephan, IEEE J. Quantum Electron. **QE-27**, 1910 (1991); M. Le Flohic, Ph.d. thesis, CNET Lannion, France, 1991; (b) E. Lacot, F. Stoeckel, and M. Chenevier, Phys. Rev. A **49**, 3997 (1994); E. Lacot, Ph.D. thesis, Université J. Fourier, Grenoble, France, 1992.

[15] K. Arai, H. Namikawa, K. Kumata, and T. Honda, J. Appl. Phys. **59**, 3430 (1986).

[16] D. W. Hall, R. A. Haas, W. F. Krupke, and M. J. Weber, IEEE J. Quantum Electron. **QE-19**, 1704 (1983).

[17] H. Rawson, *Inorganic Glass Forming Systems* (Academic, London, 1967), p. 317.

[18] R. H. Stolen, Opt. Lett. **12**, 585 (1987).

[19] C. L. Tang, H. Statz, and G. De Mars, J. Appl. Phys. **35**, 1377 (1964); Paul Mandel and G. P. Agrawal, Opt. Commun. **42**, 269 (1982); Paul Mandel and N. B. Abraham, Opt. Commun. **51**, 87 (1984); C. Etrich, Paul Mandel, N. B. Abraham, and H. Zeghlache, IEEE J. Quantum Electron. **QE-28**, 811 (1992).

[20] J. T. Lin, P. R. Morkel, L. Reekie, and D. N. Payne, *Proceedings of ECOC'87, Helsinki, Finland, 1987* (ECOC, Helsinki, 1987), Vol. I, pp. 109–112; J. T. Lin, W. A. Gambling, and D. N. Payne, *Proceedings of CLEO'89, Baltimore, 1989* (CLEO, Baltimore, 1989), Vol. I, pp. 90–91; J. T. Lin and W. A. Gambling, *Proceedings of IEEE Colloquium '90*, London, 1989 (IEEE, London, 1989), p. 10.

[21] H. Zeghlache, P. Mandel, N. B. Abraham, L. M. Hoffer, G. L. Lippi, and T. Mello, Phys. Rev. A **37**, 470 (1988).